LIMNOLOGY
and
OCEANOGRAPHY

ASLO

Limnol. Oceanogr. 60, 2015, 497–511

doi: 10.1002/lno.10045

Attenuation of diffusive noble-gas transport in laminated sediments of the Stockholm Archipelago

Yama Tomonaga,*[1,2,3] Matthias S. Brennwald,[1] Rolf Kipfer[1,2,4]

[1]Eawag, Swiss Federal Institute of Aquatic Science and Technology, Department of Water Resources and Drinking Water, CH-8600 Dübendorf, Switzerland

[2]Institute of Biogeochemistry and Pollutant Dynamics, Department of Environmental Systems Science, Swiss Federal Institute of Technology (ETH), CH-8092 Zurich, Switzerland

[3]Atmosphere and Ocean Research Institute, The University of Tokyo, 5-1-5 Kashiwanoha, Kashiwa-shi, Chiba 277-8564, Japan

[4]Institute of Geochemistry and Petrology, Department of Earth Sciences, Swiss Federal Institute of Technology (ETH), CH-8092 Zurich, Switzerland

Abstract

A sediment core has been sampled at a spatial resolution of about two centimeters for noble-gas analysis of the sediment pore water. This high-resolution sampling allowed an excess of dissolved atmospheric gases to be identified in the pore water at a sediment depth of 40 cm. Sedimentological evidence indicates that the observed gas excess is related to a past mass movement that trapped and conserved the gas surplus for more than a century. The measured noble-gas concentrations support the hypothesis that, depending on the sediment texture or particular structures in the sediment, the transport of noble gases in the pore space can be significantly attenuated compared to molecular diffusion in bulk water. The atmospheric noble-gas abundance in the pore water allows the deposition of sediments originally located near the air/water interface to be identified. Although the nature of the physical processes that limit the fluid transport in the pore space could not be fully assessed, our observations indicate that noble-gas concentration profiles can be archived for unexpectedly long times in specific sedimentary sequences. This finding represents a significant step forward in the interpretation of noble-gas concentrations in sediment pore waters in terms of past environmental conditions.

The concentrations of noble gases dissolved in the pore water of unconsolidated lake sediments have been shown to agree with those measured in the overlying water column (Brennwald et al. 2003, 2013). In lakes and in the ocean, the concentrations of dissolved noble gases in the water column are generally found to be in atmospheric equilibrium with respect to the temperature (T) and salinity (S) conditions prevailing during gas/water partitioning at the water surface (Aeschbach-Hertig et al. 1999; Kipfer et al. 2002). This has allowed measurements of the concentrations of atmospheric noble gases dissolved in sediment pore water to be used successfully to reconstruct the physical conditions characterizing the deep water of lakes in the past (Brennwald et al. 2004, 2005, 2013; Tomonaga et al. 2012, 2014). In such reconstructions, changes in noble-gas concentrations are interpreted in terms of changes in the physical conditions prevailing in the water column in response to climate forcing.

*Correspondence: tomonaga@eawag.ch

The transport of solutes, such as noble gases, within the pore space can be described in terms of advection and diffusion in the bulk sediment (Berner 1975; Imboden 1975; Strassmann et al. 2005), where the upper boundary condition at the sediment-water interface is given by the solute concentrations in the overlying water body. In general, the diffusive transport within a connected pore space is expected to smooth the original concentration signals in the sediment column. Therefore, the use of noble gases (as well as other species dissolved in the pore water) as proxies to reconstruct past environmental conditions may become very limited as long as the solute transport over long time scales smooths pore water concentration signals. Earlier case studies on lacustrine sediments show, however, that past noble-gas concentrations can be conserved for a long time (up to $\approx$ 10 kyr) in the pore space without being subject to significant diffusive exchange (Brennwald et al. 2004, 2005; Strassmann et al. 2005; Tomonaga et al. 2014).

Recently, Brennwald et al. (2013) summarized different conceptual hypotheses to explain the strong attenuation of diffusive exchange in the pore water. So far, this has been

attributed to: (1) the formation of new minerals or the geometric realignment of the sediment grains (e.g., Horseman et al. 1996) and the related Renkin effect (i.e., the increase in water viscosity close to the pore walls; Renkin 1954; Grathwohl 1998; Schwarzenbach et al. 2003; Brennwald et al. 2004); (2) the existence of "dead" pores that are not connected to the main pore space and the consequent entrapment of solutes (e.g., Grathwohl 1998); (3) the adsorption to the sediment matrix (Pitre and Pinti 2010); (4) and, in the case of (noble) gases, the presence of macroscopic gas bubbles that act as immobile gas reservoirs. However, as a consequence of the lack of experimental evidence, the mechanisms that lead to the observed attenuation are still not well understood.

The vertical resolution of previously published noble-gas data from unconsolidated sediments exceeds 10 cm, and previous studies have focused on sites with low sedimentation rates (< 0.1 cm yr ^{1}; e.g., Tomonaga et al. 2011*b*, 2012). The coarseness of the temporal resolution thus achieved (several centuries) has prevented the study of noble-gas concentration changes occurring on decadal timescales. Thus, a higher sampling resolution is needed to interpret the short-term temporal evolution of noble-gas concentration signals in the pore water. In particular, a higher resolution is necessary to assess whether the concentration profiles are smoothed by diffusive transport, and, if so, to what extent.

In this work, we present noble-gas concentrations and isotope ratios measured in 40 samples from a sediment core taken in the Stockholm Archipelago. The samples were taken at 23 different sediment depths separated by vertical intervals of about two centimeters. Combined with a locally high sedimentation rate (up to 2 cm yr ^{1}), this high-resolution sampling allowed us to characterize solute transport on a decadal time scale. Our data add new experimental evidence supporting the possibility of (strong) attenuation of effective noble-gas diffusion in the pore space under specific conditions. To our knowledge, this is up to now the most convincing case study showing that diffusive exchange in pore water space of unconsolidated sediments can be strongly reduced. Based on the noble-gas data and the sedimentological properties of the investigated sediments, we formulate a case specific hypothesis on the mechanisms responsible for the observed attenuation of diffusivity.

The noble-gas concentration profiles observed in this study are partly in contradiction with the predictions of the conventional models for the solute transport in the pore space. The disagreement of observed data and model predictions, therefore, stimulates a critical discussion on the completeness and validity of the assumptions underlying the conventional solute transport models in unconsolidated sediments. Our findings add further convincing evidence that noble gases dissolved in the pore water have a great potential as proxies to reconstruct palaeoenvironmental conditions in lakes and in the ocean.

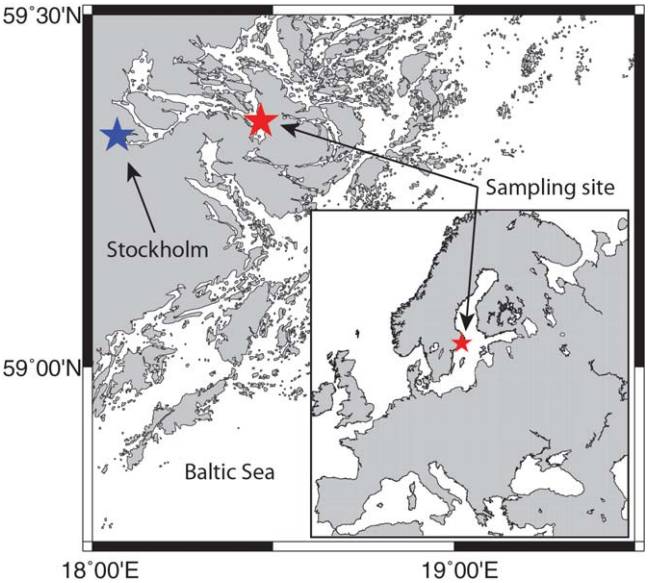

Fig. 1. Location of the sampling site in the Stockholm Archipelago (red star). The city of Stockholm is indicated by a blue star. The inset map shows an overview of Western Europe.

Methods

Study site

The Stockholm Archipelago (Sweden) constitutes a geomorphological transition zone between the lake-rich terrain of Scandinavia and the Baltic Sea (Fig. 1). In the semienclosed bays of this region, local conditions favor the inflow and retention of settling particles, leading to very high sedimentation rates of several centimeters per year (Meili et al. 2000). The undisturbed accumulation of sediment (especially in the deep regions) allows annual varves to form with thicknesses of up to five centimeters (Meili et al. 2000; Persson and Jonsson 2000).

At the chosen sampling location of 59°20.99′N/18°27.94′E (36 m water depth), a maximum varve thickness of about two centimeters was determined by optical inspection of the uppermost 12 cm of the sediment column. Within the uppermost 15 cm, the sediment shows only slight layering, and the water content is high ($> 90\%$) due to incomplete compaction (Fig. 2).

The extremely high sedimentation rates easily allowed the annual depositions to be distinguished macroscopically (i.e., using the colors of the different layers). A sedimentological disturbance, manifested as an abrupt change of the appearance (and texture) of the sediment, was clearly visible at a depth of 40 cm in the core. Compared to the laminated structure of the overlying sediment column, the sediment below 40 cm is characterized by a lighter color, a more homogeneous texture, and lower porosity (*see* Fig. 2). A first estimate of the age of the sediment layers obtained by varve counting (Fig. 2) identified the sedimentological disturbance

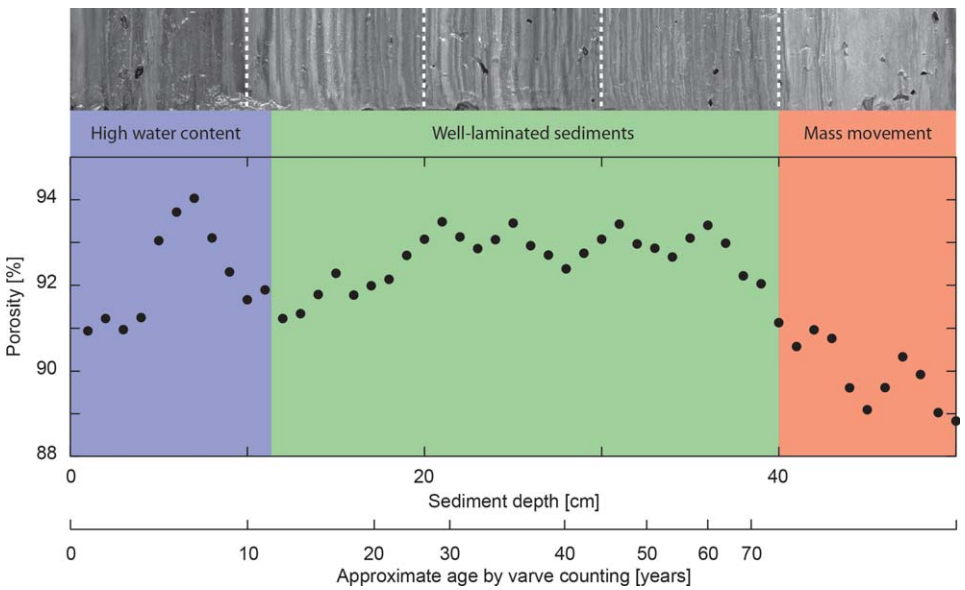

Fig. 2. Macroscopic structure and porosity profile determined for the sediments at the noble gas sampling station in the Stockholm Archipelago. In the topmost 12 cm of the sediment (blue), annual laminations are present, but lamination is not as well defined as in deeper parts of the sediment column. The relatively low porosity in the first 5 6 cm of sediment may be an artifact caused by water loss from the liner during transport from Swe den to Switzerland. In the middle part of the sediment column (green) annual laminations can be clearly observed and the porosity is virtually con stant within ± 2%. Below 40 cm depth (red) evidence of a mass movement is present: the sediment color is lighter, the porosity decreases with depth to below 91%, and no lamination is visible. The age scale is based on optical varve counting which is confirmed by ^{137}Cs and ^{210}Pb dating.

to be older than 80 yr. However, as the laminations in the upper part of the core are not completely undisturbed, we also used radiometric ^{137}Cs and ^{210}Pb dating to determine reliably the age of the disturbance.

Noble-gas sampling and analysis

A 1.03-m-long sediment core taken by a gravity corer was sampled for noble-gas analysis using the method of Brennwald et al. (2003). Bulk sediment was transferred from the plastic liner containing the core into small copper tubes which were closed air-tight with two special metal clamps (Brennwald et al. 2003; Tomonaga et al. 2011*a*).

The samples were taken at vertical intervals of approximately two centimeters. The distance between adjacent samples approaches the geometrical limits of the adopted sampling technique (Brennwald et al. 2003). Because of geometrical constraints it is questionable whether samples taken at intervals of less than two centimeters would belong to the depth at which the copper tube samplers are attached to the core liner. To fill a larger number of samplers, more bulk-sediment volume is required. During the transfer of the sediment into the copper tube samplers, two pistons push the core material out of the liner simultaneously from both sides (Brennwald et al. 2003; Tomonaga et al. 2011*a*). As the uppermost part of the sediment column normally shows a strong porosity gradient (i.e., the porosity decreases with depth), and as sediment of higher porosity often flows more easily than sediment of lower porosity, the upper samplers tend to be filled with sediment before the bottom samplers. The bottom samples are, therefore, filled and closed after a certain volume of bulk sediment has already, preferentially, left the plastic liner from the upper part of the sediment core. If this volume exceeds the volume of bulk sediment present between each sampling depth, it is possible that the uncertainty in the effective sampling depth for the bottom samples encompasses the depths of the adjacent samples; i.e., the depth resolution in the lower part of the core is coarser than in the upper part. Moreover, as the squeezing procedure can displace the original position of the liner with respect to the frame holding the core with the inserted pistons, a shift of a few millimeters is normal, but this shift can be greater if more sediment volume is needed to flush and fill more samplers. Access to the metal clamps (≈ 4 cm width), which need to be tightly closed to seal the copper tubes, must also be guaranteed. Removal of the copper tubes from the liner to close the clamps is not an option as contamination of the remaining samples with air would likely occur.

A total of 40 samples from 23 different sampling depths was collected from a single sediment core. During the sampling procedure, the observed displacement of the plastic liner with respect to the holding frame during the squeezing procedure was ≈ 1 cm. This observation, taken together with the calculated amount of sediment volume pushed out of the core to fill the samples, yields uncertainties of ± 0.5 cm to ± 3.3 cm for the acquisition depth of the samples.

Table 1. Measured concentrations, isotope ratios, concentrations corrected for degassing and respective uncertainties at the 1-σ eve for samp es from the Stockho m Archipe - ago. For some samp es redetermination of nob e gas abundances a owed the exc usion of measurements where air contamination was suspected (these samp es are identified by a 5-digit fina number). STP = standard temperature (0°C) and pressure (1 atm).

Sample	z (m)	Concentrations ($cm^3STP\ g^{-1}$)					Isotope ratios			Corrected concentrations ($cm^3STP\ g^{-1}$)			
		He	Ne	Ar	Kr	Xe	$^3He/^4He$	$^{20}Ne/^{22}Ne$	$^{36}Ar/^{40}Ar$	He	Ar	Kr	Xe
		10^{-8}	10^{-7}	10^{-4}	10^{-7}	10^{-8}	10^{-6}		10^{-3}	10^{-8}	10^{-4}	10^{-7}	10^{-8}
Saturation concentration		4.49	2.19	4.12	1.00	1.50	(calculated for $T = 4$ C and $S = 11$ g kg^{-1})						
SE,331,2867	0 02±0 01	5 81±0 05	2 04±0 02	4 37±0 04	1 06±0 01	1 72±0 03	1 19±0 01	9 76±0 02	3 390±0 002	6 6±0 1	4 55±0 05	1 09±0 01	1 76±0 03
SE,331,2877	0 04±0 01	6 54±0 06	2 00±0 02	4 27±0 04	1 04±0 01	1 68±0 02	1 04±0 02	9 79±0 01	3 383±0 003	7 6±0 1	4 50±0 05	1 07±0 01	1 72±0 03
SE,331,28771	0 04±0 01	6 51±0 06	2 01±0 02	4 46±0 04	1 10±0 01	1 78±0 02	1 07±0 01	9 78±0 01	3 379±0 001	7 6±0 1	4 69±0 05	1 14±0 01	1 82±0 03
SE,331,28641	0 06±0 01	7 24±0 06	1 93±0 02	4 44±0 04	1 09±0 01	1 73±0 02	1 06±0 01	9 79±0 01	3 385±0 002	8 9±0 2	4 77±0 05	1 14±0 01	1 79±0 03
SE,331,2885	0 08±0 01	7 15±0 06	1 92±0 02	4 10±0 03	0 98±0 01	1 55±0 02	0 96±0 02	9 82±0 01	3 387±0 003	8 9±0 2	4 42±0 04	1 03±0 01	1 61±0 02
SE,331,28851	0 08±0 01	6 98±0 07	1 96±0 02	4 35±0 04	1 07±0 01	1 67±0 02	1 01±0 02	9 76±0 01	3 383±0 002	8 4±0 2	4 64±0 05	1 11±0 01	1 72±0 03
SE,331,2887	0 10±0 01	11 6±0 1	2 24±0 02	4 30±0 03	1 01±0 01	1 57±0 02	0 74±0 01	9 79±0 01	3 386±0 001	11 6±0 2	4 30±0 04	1 01±0 01	1 57±0 02
SE,331,28871	0 10±0 01	6 63±0 06	1 29±0 01	3 44±0 03	0 91±0 01	1 55±0 02	0 70±0 01	9 78±0 01	3 385±0 002	11 9±0 2	4 33±0 04	1 06±0 01	1 75±0 03
SE,331,28711	0 12±0 01	9 10±0 08	1 85±0 02	4 07±0 03	0 98±0 01	1 61±0 02	0 76±0 01	9 77±0 01	3 382±0 003	11 9±0 2	4 47±0 05	1 05±0 01	1 69±0 02
SE,331,2863	0 14±0 01	13 0±0 1	1 92±0 02	4 23±0 04	1 04±0 01	1 64±0 03	0 64±0 01	9 79±0 01	3 385±0 002	16 1±0 3	4 56±0 06	1 09±0 01	1 70±0 03
SE,331,28631	0 14±0 01	14 8±0 2	2 27±0 03	4 83±0 05	1 18±0 01	1 86±0 03	0 61±0 01	9 81±0 01	3 381±0 003	14 8±0 4	4 83±0 06	1 18±0 01	1 86±0 03
SE,331,2882	0 16±0 01	11 1±0 1	1 56±0 02	3 51±0 03	0 90±0 01	1 53±0 02	0 58±0 01	9 76±0 02	3 385±0 002	17 3±0 3	4 15±0 05	1 00±0 01	1 66±0 03
SE,331,28821	0 16±0 01	12 7±0 1	1 83±0 02	4 12±0 05	1 02±0 01	1 66±0 03	0 55±0 01	9 80±0 01	3 384±0 002	16 7±0 4	4 54±0 06	1 09±0 01	1 75±0 03
SE,331,2891	0 18±0 01	17 5±0 2	2 33±0 03	4 67±0 04	1 11±0 01	1 73±0 03	0 54±0 01	9 83±0 01	3 387±0 002	17 5±0 4	4 67±0 05	1 11±0 01	1 73±0 03
SE,331,28911	0 18±0 02	20 3±0 2	2 66±0 03	5 44±0 06	1 30±0 01	1 99±0 03	0 56±0 01	9 80±0 01	3 381±0 002	20 3±0 5	5 44±0 06	1 30±0 01	1 99±0 03
SE,331,2894	0 20±0 02	27 4±0 3	2 52±0 03	5 55±0 06	1 37±0 02	2 15±0 04	0 46±0 01	9 83±0 01	3 391±0 003	27 4±0 7	5 55±0 07	1 37±0 02	2 15±0 03
SE,331,2879	0 22±0 02	9 33±0 09	1 08±0 01	2 73±0 03	0 74±0 01	1 32±0 02	0 47±0 01	9 81±0 02	3 384±0 003	18 6±0 3	3 61±0 04	0 89±0 01	1 53±0 02
SE,331,28791	0 22±0 02	13 3±0 1	1 39±0 02	3 91±0 04	1 07±0 01	1 80±0 03	0 48±0 01	9 81±0 01	3 382±0 004	22 7±0 4	4 81±0 05	1 23±0 01	2 01±0 03
SE,331,2890	0 24±0 02	18 2±0 2	2 04±0 02	4 67±0 05	1 20±0 01	1 96±0 03	0 46±0 01	9 81±0 02	3 384±0 002	20 6±0 5	4 87±0 06	1 23±0 02	2 00±0 03
SE,331,28901	0 24±0 02	13 7±0 1	1 52±0 02	3 71±0 04	0 98±0 01	1 66±0 03	0 48±0 01	9 816±0 005	3 386±0 002	21 8±0 4	4 42±0 05	1 10±0 01	1 82±0 03
SE,331,2892	0 26±0 02	13 6±0 1	1 41±0 02	3 77±0 04	1 03±0 01	1 74±0 03	0 48±0 01	9 85±0 01	3 381±0 004	23 1±0 4	4 62±0 05	1 18±0 01	1 93±0 03
SE,331,28921	0 26±0 02	14 7±0 2	1 66±0 02	3 97±0 04	1 05±0 01	1 75±0 03	0 45±0 01	9 80±0 02	3 383±0 003	21 7±0 4	4 58±0 06	1 16±0 01	1 89±0 03
SE,322,2883	0 28±0 02	12 8±0 1	0 98±0 01	2 97±0 03	0 87±0 01	1 55±0 02	0 43±0 01	9 83±0 03	3 390±0 005	26 6±0 4	4 01±0 05	1 06±0 01	1 82±0 02
SE,331,28831	0 28±0 02	11 4±0 1	0 99±0 01	2 83±0 03	0 80±0 01	1 46±0 02	0 42±0 01	9 81±0 02	3 384±0 004	23 5±0 4	3 81±0 04	0 98±0 01	1 71±0 03
SE,331,28781	0 30±0 02	16 0±0 2	1 50±0 02	3 76±0 04	1 00±0 01	1 69±0 03	0 42±0 01	9 78±0 02	3 382±0 002	25 9±0 4	4 52±0 05	1 13±0 01	1 86±0 03
SE,331,2895	0 32±0 02	24 5±0 3	1 93±0 02	4 46±0 05	1 19±0 01	1 98±0 03	0 40±0 01	9 81±0 01	3 385±0 003	30 1±0 7	4 79±0 07	1 25±0 02	2 05±0 03
SE,331,28951	0 32±0 02	38 9±0 6	3 13±0 05	6 75±0 10	1 72±0 03	2 71±0 05	0 399±0 005	9 82±0 01	3 383±0 002	39±1	6 8±0 1	1 72±0 02	2 71±0 05
SE,331,2881	0 34±0 02	11 1±0 1	0 64±0 01	2 13±0 02	0 66±0 01	1 28±0 02	0 36±0 01	9 86±0 04	3 391±0 005	26 4±0 4	3 08±0 04	0 85±0 01	1 56±0 03
SE,331,28721	0 36±0 03	11 6±0 1	0 83±0 01	2 59±0 03	0 77±0 01	1 40±0 02	0 38±0 01	9 85±0 03	3 394±0 004	25 7±0 4	3 60±0 04	0 96±0 01	1 67±0 03
SE,331,2886	0 38±0 03	23 8±0 3	1 23±0 02	3 43±0 04	1 01±0 01	1 76±0 03	0 304±0 005	9 86±0 03	3 389±0 004	44 2±0 8	4 38±0 06	1 19±0 02	2 00±0 03
SE,331,2884	0 40±0 03	76±1	2 78±0 05	7 4±0 1	2 11±0 03	3 43±0 07	0 24±0 01	9 84±0 01	3 392±0 004	76±2	7 4±0 1	2 11±0 03	3 43±0 06
SE,331,28841	0 40±0 03	55 5±0 7	1 97±0 03	5 87±0 08	1 72±0 02	2 80±0 05	0 27±0 01	9 85±0 01	3 390±0 001	66±2	6 2±0 1	1 78±0 03	2 89±0 05
SE,331,2873	0 42±0 03	15 7±0 2	0 85±0 01	2 61±0 03	0 78±0 01	1 42±0 02	0 33±0 01	9 88±0 03	3 390±0 005	34 4±0 5	3 62±0 04	0 97±0 01	1 69±0 03
SE,331,28731	0 42±0 03	21 2±0 3	1 21±0 02	3 44±0 04	1 01±0 01	1 77±0 03	0 34±0 01	9 85±0 02	3 389±0 002	39 8±0 8	4 41±0 06	1 19±0 02	2 02±0 03
SE,331,2875	0 44±0 03	72±1	2 65±0 04	7 1±0 1	1 95±0 03	3 11±0 06	0 27±0 01	9 86±0 01	3 393±0 002	72±2	7 1±0 1	1 95±0 03	3 11±0 05
SE,331,28751	0 44±0 03	30 6±0 4	1 14±0 02	3 48±0 04	1 05±0 01	1 80±0 03	0 266±0 004	9 87±0 02	3 391±0 002	59±1	4 54±0 07	1 25±0 02	2 06±0 04
SE,331,2876	0 46±0 03	58 7±0 7	2 35±0 03	5 83±0 07	1 62±0 02	2 60±0 04	0 27±0 01	9 85±0 01	3 387±0 002	59±2	5 83±0 08	1 62±0 02	2 60±0 04
SE,331,28761	0 46±0 03	78±1	2 94±0 04	7 2±0 1	2 00±0 03	3 21±0 06	0 254±0 005	9 88±0 01	3 391±0 001	78±2	7 2±0 1	2 00±0 03	3 21±0 05
SE,331,2870	0 48±0 03	116±2	4 26±0 07	9 1±0 2	2 46±0 04	3 80±0 08	0 266±0 005	9 86±0 01	3 395±0 001	116±4	9 1±0 1	2 46±0 03	3 80±0 06
SE,331,28701	0 48±0 03	186±4	6 9±0 1	14 7±0 3	3 93±0 08	5 9±0 1	0 267±0 004	9 866±0 004	3 390±0 002	186±15	14 7±0 2	3 93±0 04	5 90±0 06
Average error (%)		1.1	1.2	1.1	1.2	1.6	1.6	0.2	0.1	2.2	1.2	1.2	1.6

The noble-gas abundances in the pore waters were determined by the extrusion method of Brennwald et al. (2003) at the Noble Gas Laboratory of the Swiss Federal Institute of Science and Technology (ETH) in Zurich. Technical details concerning the gas purification line and the mass spectrometric noble-gas determination are described in Beyerle et al. (2000). The analytical protocol used yields He, Ne, Ar, and Kr concentrations with an overall error of 1.2%, and Xe concentrations with a slightly higher error of 1.6% (Table 1; for more details on the applied methods *see* Brennwald et al. 2003, 2013).

^{137}Cs and ^{210}Pb dating and sediment porosity

A second sediment core was recovered at the same location as the core used for noble-gas analysis. This second core was opened and cut vertically into two halves. One half was used to visually inspect the macroscopic structure of the sediment column (e.g., for annual lamination and mass movements, *see* Fig. 2). The other half was sampled at vertical intervals of one centimeter for ^{137}Cs and ^{210}Pb dating to determine the age of the sediment (Pennington et al. 1973; Ritchie et al. 1973; Appleby and Oldfield 1978; Appleby 2001).

To determine the ^{137}Cs and ^{210}Pb activities, the sediment samples were vacuum dried. From the weight difference before and after desiccation, the porosity profile of the sediment column at the sampling site was reconstructed (Fig. 2). We assumed a solid-sediment density of 2.6 g cm ^{3} (quartz) to calculate the porosity. Note that the true porosity may be lower than the calculated values because the sediments of the Stockholm Archipelago are rich in organic matter, which in general shows a lower solid-sediment density. However, this porosity bias does not affect the further interpretation of the porosity profile and the modeling of solute transport.

The sediment porosity is not only useful to characterize the transport of dissolved gases within the pore space but it can also be used as a simple and straightforward parameter to detect structural changes in the sediment matrix. For instance, the textural change at 40 cm sediment depth is characterized by a distinct change in porosity and in water content (Fig. 2).

Diffusion model

An advection/diffusion model describing the vertical transport equation for nonreactive solutes (Strassmann et al. 2005) was used to determine the most relevant transport parameters, such as the effective diffusivities, that control the migration of noble gases (and other solutes) in the connected pore space of the sediment column (for similar approaches *see* Berner 1975; Imboden 1975):

$$\phi \frac{\partial C_i}{\partial t} \quad \frac{\partial}{\partial z}\left(\phi D_{\mathrm{eff},i} \frac{\partial C_i}{\partial z}\right) \quad U\phi \frac{\partial C_i}{\partial z} + \phi r \tag{1}$$

$$D_{\mathrm{eff},i} \quad \frac{\phi}{a} D_{\mathrm{mol},i} \tag{2}$$

where C_i is the concentration of the dissolved noble gas i He, Ne, Ar, Kr, Xe, ϕ is the porosity, U is the vertical pore water velocity (advective term), r is a source term (in our modeling we set r 0). The effective diffusivity, $D_{\mathrm{eff},i}$, was parameterized by the molecular diffusivity of noble gases in free water, $D_{\mathrm{mol},i}$, and the porosity, ϕ, being scaled by the dimensionless factor a. Note that in principle $D_{\mathrm{eff},i}$ includes all the possible processes affecting the solute diffusion in the pore space. Therefore, in contrast to many other sediment transport models where the parameter a reflects tortuosity only, we use a here as a scaling parameter that covers and integrates all processes that may attenuate solute diffusion within the pore water on a macroscopic level. This includes tortuosity but also includes solute retention caused by doubly porous media, sorption or trapping of solutes in dead pores or gas bubbles, or any other unidentified process attenuating (macroscopic) diffusion (Brennwald et al. 2013).

A continuous, time-independent function for porosity at different sediment depths was constructed by linear interpolation of the calculated porosity profile (spatial resolution of approximately one centimeter). For sediment depths $>$ 0.5 m a constant porosity of 89% (i.e., the lowest porosity determined in the core) was assumed.

Results

Noble-gas profile in the pore water of the sediment column

Table 1 lists, for all 40 samples collected in the Stockholm Archipelago, the measured noble-gas concentrations for He, Ne, Ar, Kr, and Xe as well as the ^{3}He/^{4}He, ^{20}Ne/^{22}Ne, and ^{36}Ar/^{40}Ar ratios and their average overall experimental errors. The results are plotted in Fig. 3 as relative concentrations normalized by the expected concentrations and isotope ratios of air-saturated water for local temperature and salinity conditions (T 4°C and S 11 g kg ^{1}). It should be noted that the concentration differences in replicate samples taken at the same sediment depth (e.g., at 32 cm, 40 cm, 44 cm, 46 cm, or 48 cm depth) are the result of the strong vertical concentration gradients and the slight vertical offset of the replicates caused by squeezing the sediment during sampling (*see* the Methods section).

Between 0 cm and 40 cm depth the concentrations of all atmospheric noble gases (Ne Xe) approach the expected saturation concentrations and remain more or less constant. Constant noble-gas concentrations close to the expected equilibrium concentrations indicate the undisturbed embedding of water from the sediment/water interface in the sediment pore space (Brennwald et al. 2003; Strassmann et al. 2005).

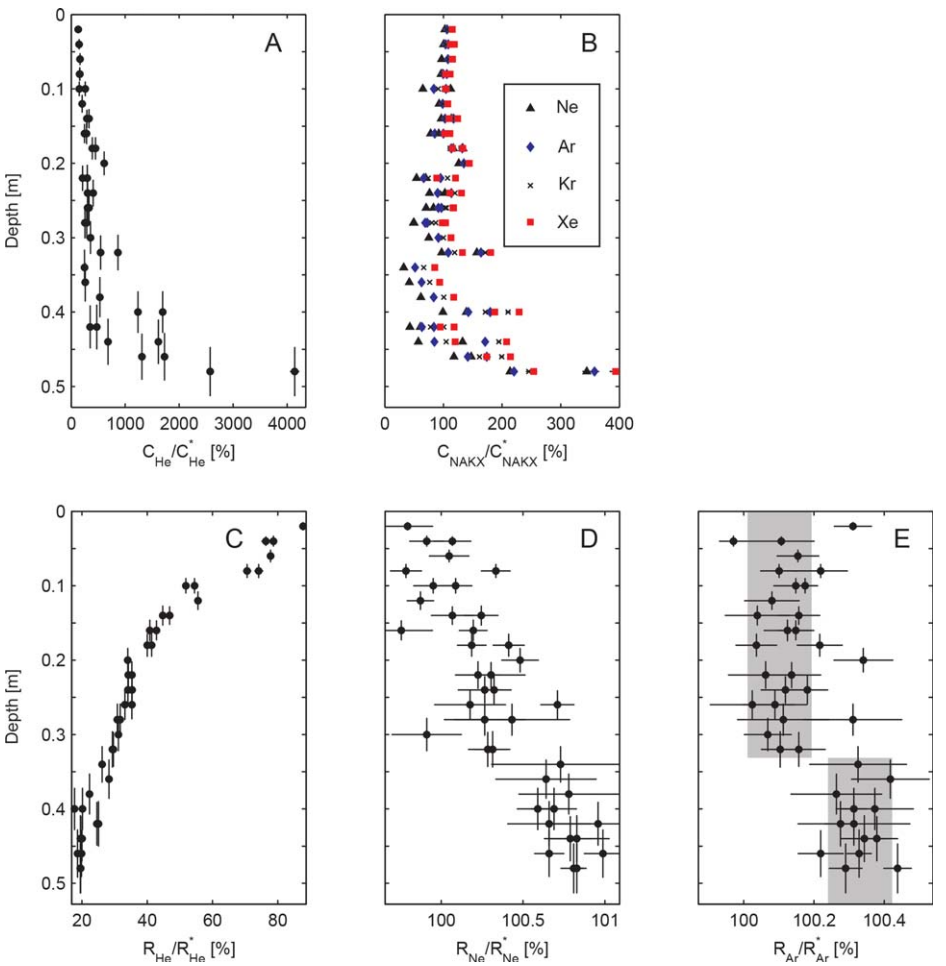

Fig. 3. Noble gas concentrations and isotope ratios relative to the expected equilibrium values for ASW (air saturated water; T 4°C and S 11 g kg ^{1}). C_i: measured concentration of species i (with i He, NAKX). NAKX Ne (black triangles), Ar (blue diamonds), Kr (black crosses), and Xe (red squares). C_i^*: ASW concentration of species i; R_{He}: measured $^3He/^4He$ ratio; R^*_{He}: $^3He/^4He$ ratio of ASW; R_{Ne}: measured $^{20}Ne/^{22}Ne$ ratio; R^*_{Ne}: $^{20}Ne/^{22}Ne$ ratio of ASW; R_{Ar}: measured $^{36}Ar/^{40}Ar$ ratio; R^*_{Ar}: $^{36}Ar/^{40}Ar$ ratio of ASW. Note that for clarity, the depth uncertainties for the NAKX concentrations are not plotted; they are the same as those for the He concentrations. The errors are in general smaller than the plotted symbols (Table 1). The gray areas (meant as a visual aid with no statistical meaning) underline the sudden increase in the $^{36}Ar/^{40}Ar$ isotope ratios in the depth range characterized by the presence of a mass movement.

The He concentration increases slightly with depth (Fig. 3A) due to the accumulation of terrigenic He, which is either produced in situ by the radioactive decay of Th and U in the sediment matrix, or is injected from deeper strata (Dyck and Da Silva 1981; Stephenson et al. 1994; Ballentine et al. 2002; Brennwald 2004).

Some samples seem to have been affected by degassing during sampling. In these samples, the Ne concentrations (Fig. 3B, black triangles) are lower (< 80%) than the expected saturation concentration. With increasing atomic mass (from Ar to Xe), the deviations of the measured noble-gas concentrations relative to the expected equilibrium concentrations generally decrease, as the more soluble heavier (noble) gases are less subject to secondary gas exchange (Kipfer et al. 2002; Holzner et al. 2008). This systematic noble-gas depletion pattern is indicative of degassing processes (Brennwald et al. 2005). Again, we note that the samples from the lower part of the sediment core were collected after the ones at the top. We, therefore, assume that the observed degassing occurred during the sampling process (which lasted more than 30 min) because of the formation of gas bubbles in the sediment core as a result of the decrease in pressure during the recovery of the core. However, such degassing processes only lower the measured noble-gas concentrations; from this point of view the concentrations given in Table 1 are minimum estimates.

Below 40 cm depth we observed strong fluctuations in concentration, with substantial supersaturations of all noble gases, both atmospheric and nonatmospheric. In contrast to the upper part of the sediment column, where the measured

concentrations of the atmospheric noble gases agree reasonably well with the expected equilibrium concentrations, the sediment below 40 cm depth is characterized by supersaturations of up to 200-400% (Fig. 3B). As atmospheric noble gases enter meteoric water only by air/water partitioning, the atmospheric noble-gas surpluses can only be explained by the trapping of significant volumes of atmospheric air (e.g., Kipfer et al. 2002; Aeschbach-Hertig and Solomon 2013).

In contrast to the supersaturations measured in the pore water by Pitre and Pinti (2010), noble-gas adsorption on to sediment particles cannot account for the gas excesses observed here. First, in the case of the noble-gas profile from the Stockholm Archipelago, the extent of the supersaturation observed is similar for all atmospheric noble-gas species (i.e., the excess has a noble-gas signature similar to atmospheric air). Second, as discussed in more detail below, Ne and Ar are enriched in light isotopes. Third, the He excesses are one order of magnitude larger than the excesses of Ne, Ar, Kr, and Xe. All these facts negate adsorption as the cause of the observed noble-gas surpluses, as adsorption generally favors the enrichment of heavy elements and isotopes (Podosek et al. 1980, 1981; Mamyrin and Tolstikhin 1984; Ozima and Podosek 2002).

Further, the observed supersaturations cannot be related to air contamination during the sampling process, as the $^{3}He/^{4}He$, $^{20}Ne/^{22}Ne$, and $^{36}Ar/^{40}Ar$ ratios would evolve toward the equilibrium values for air-saturated water a trend that is not observed (Fig. 3C E).

Because of the presence of atmospheric noble-gas excesses, the textural change at a sediment depth of 40 cm (Fig. 2) is interpreted as the result of a mass movement that originated from near-surface regions (e.g., the shore). The mass movement seems to have entrained air that has been deposited and trapped in the bulk sediment of the Stockholm Archipelago. From the observation of free gas phases in the sediments of Lake Van (Turkey) using seismic profiling Cukur et al. (2013) concluded that abrupt changes in the sediment texture such as turbidites and deltaic deposits have the potential to provide ideal conditions to allow the sediments to act as an effective gas reservoir.

The $^{20}Ne/^{22}Ne$ and $^{36}Ar/^{40}Ar$ ratios in the mass movement are higher (approximately 0.8% and $\approx 0.3\%$, respectively) than in the upper part of the sediment column where the noble-gas concentrations are very similar, or agree with the respective atmospheric equilibrium ratios for air-saturated water (Beyerle et al. 2000). The depth at which enrichment of the light ^{20}Ne and ^{36}Ar isotopes occurs (Fig. 3E, gray areas) agrees well with the depth of the change in sediment texture (Fig. 2). The slight geometrical offset between the gas anomaly and the textural change may be related to the spatial heterogeneity of the mass movement (i.e., the thickness of the disturbance may be different in space) or to the advective pore-water displacement relative to the sediment matrix due to compaction of the bulk sediment (Berner 1975; Imboden 1975; Strassmann et al. 2005).

Conceptually, the enrichment of the light noble-gas isotopes can be understood as kinetic fractionation during gas/water partitioning, which can be described by a Rayleigh process (Holocher et al. 2003; Brennwald et al. 2005; Zhou et al. 2005; Klump et al. 2007, 2008; Tyroller et al. 2014). At the time of deposition of the mass movement, atmospheric air bubbles were entrained into the moving mass of water and sediment. During the descent toward the bottom of the basin, the lighter isotopes fractionated faster into the water phase than the heavier isotopes, because their molecular diffusivity is slightly higher.

It appears most reasonable to us that during a turbulent event such as a mass movement, the dissolution of entrapped air bubbles will not be complete; for example, some of the air bubbles might escape toward the water/air interface. Under such circumstances, a slight enrichment of the dissolved gas phase with light isotopes can be expected, as the escaping gas bubbles are enriched in heavier isotopes that dissolve at a slower rate during the kinetic gas partitioning process.

The He concentrations in the deeper part of the core significantly exceed the concentrations measured in the upper part of the sediment column close to the sediment/water boundary. In contrast to the other noble gases, which are of purely atmospheric origin, the He excess is one order of magnitude larger.

The $^{3}He/^{4}He$ isotope ratio in the pore waters is lower than that of air-saturated water ($^{3}He/^{4}He \quad 1.36 \times 10^{-6}$, Weiss 1970) throughout the entire sediment core, which indicates that isotopically heavy terrigenic He accumulates in the sediment pore water. The isotope ratio of the excess He in the bottom samples ($^{3}He/^{4}He \approx 2.3 \times 10^{-7}$) is significantly higher than that determined in the North Sea ($^{3}He/^{4}He \approx 1.45 \times 10^{-7}$, Oxburgh et al. 1986). The higher ratios are attributed to the atmospheric He excess originating from the mass movement ($^{3}He/^{4}He_{atm} > {}^{3}He/^{4}He_{terr}$). The $^{3}He/^{4}He$ ratio of terrigenic He can be estimated by subtracting the atmospheric $^{(3,4)}He$ excess which can be assumed to be proportional to the Ne excess (with respect to the expected saturation concentration). The fractionation of the He isotopes at the time of deposition of the mass movement (i.e., similarly to the Ne and Ar isotopes) is expected to be negligible, as the abundance of terrigenic He is about one order of magnitude higher than the He excess originating from the atmosphere (assuming that the atmospheric He excess is similar to the excess observed for the purely atmospheric noble gases; Fig. 3B). In fact, a hypothetical fractionation of the $^{3}He/^{4}He$ ratio in the atmospheric excess of 2% (i.e., a value higher than the one expected for the fractionation of the He isotopes of approximately 1.4% considering a linear relationship between atomic mass and fractionation percentage observed for the Ne and Ar isotopes) would result

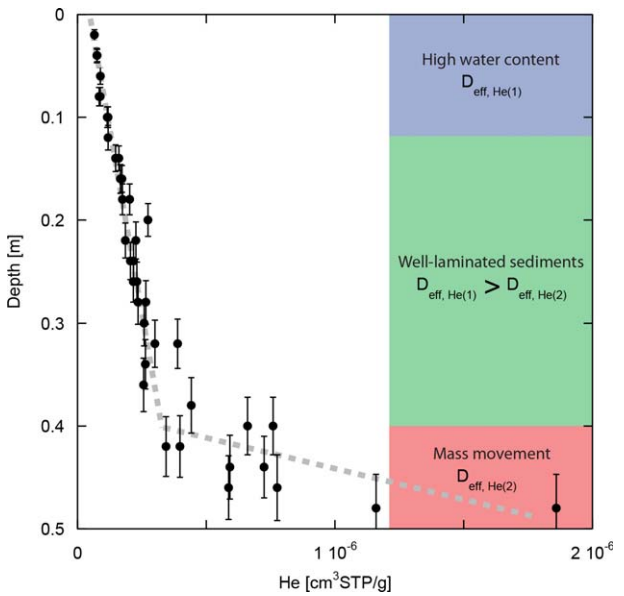

Fig. 4. He concentration profile corrected for degassing effects. The amount of "degassed" He was calculated from the Ne depletion with respect to the expected atmospheric equilibrium concentration multiplied by a factor $D_{mol,He}/D_{mol,Ne}$ (i.e., the degassing process is diffusion limited). The corrected He profile shows two intervals with different diffusive behavior (i.e., with different effective diffusivities, $D_{eff,He(1)}$ and $D_{eff,He(2)}$). The colored areas on the right hand side of the figure correspond to the macroscopic structure and porosity sections of Fig. 2.

in a difference of only about 1% in the corrected $^3He/^4He$ ratio for terrigenic He. Tritiogenic ^3He produced by the decay of ^3H is negligible, because the concentration of ^3He produced by the decay of water with 5 TU (i.e., the ^3H concentration before the nuclear tests in the 1960s) is more than one order of magnitude smaller than the measured ^3He concentrations. The correction for the atmospheric He excess results in $^3He/^4He \approx 1.5 \times 10^{-7}$ for the terrigenic He component in the mass movement, which agrees closely with the isotope signature of terrigenic He in the North Sea (Oxburgh et al. 1986).

The presence of large amounts of terrigenic He below 40 cm depth suggests that the mass movement forms a barrier where the effective He diffusivity is considerably lower than in the laminated sediment above. This layer strongly attenuates the upward diffusion of solutes emanating from deeper strata, which results in accumulation of terrigenic He in the pore water.

Assuming that Ne degassing during sampling is a diffusion-controlled process, the measured He concentrations can be corrected by adding the "degassed" He component, which is proportional to the respective Ne depletion multiplied by a factor $D_{mol,He}/D_{mol,Ne}$. The He concentration profile corrected for degassing is shown in Fig. 4 and Table 1 (where the corrected concentrations for Ar, Kr, and Xe are also listed). Compared to the uncorrected data, the corrected He concentration profile is more homogeneous and less scattered. In particular, the concentrations of samples taken at the same sediment depth tend to be more consistent with each other (which supports the validity of the applied correction). Between 0 cm and 40 cm depth the corrected He concentration increases linearly with depth (with a concentration gradient $\partial C_{He}/\partial z \approx 8.1 \times 10^{-9}$ cm^{3}STP g^{-1} cm^{-1}). From a depth of 40 cm, the He concentration profile is characterized by a much stronger concentration gradient ($\partial C_{He}/\partial z \approx 95 \times 10^{-9}$ cm^{3}STP g^{-1} cm^{-1}), as already observed in the non-corrected profile. The upward flux of terrigenic He is given by Fick's Law ($j_{He} \quad D_{eff,He} \cdot \partial C_{He}/\partial z$). Neglecting the in situ production of terrigenic He by the radioactive decay of U and Th isotopes, the He flux can be considered constant throughout the entire sediment core. The larger He concentration gradient below 40 cm, therefore, indicates that the effective He diffusivity in the mass movement is much less than in the overlying sediment.

Sediment dating and porosity

To assess the temporal evolution of dissolved noble gases in the pore water, we dated the sediments using ^{137}Cs and ^{210}Pb. The measured activities and the estimated ages for both isotopes are given in Table 2. In the upper part of the core, the ^{137}Cs and ^{210}Pb ages tend to agree with each other. In the lower part of the sediment core, the ^{210}Pb ages are generally lower than the ^{137}Cs ages although both age estimates agree within 25%. The lower ^{210}Pb ages most likely result from uncertainties in the correction of the measured ^{210}Pb activities for the in situ production of ^{210}Pb in the sediment grains (Table 2).

The two ^{137}Cs activity maxima for 1986 (Tschernobyl) and the 1960s (atomic bomb tests) are found within the sampled depth range at 12 cm and 24 cm. The ^{137}Cs activities (Fig. 5) are highly compatible with the varve chronology. We, therefore, used the ^{137}Cs results as a rough estimate to reconstruct the sedimentation history.

By linearly extrapolating the sediment age-depth relationship defined by the ^{137}Cs peaks corresponding to 1986 and the 1960s, the age of the mass movement is estimated to be older than 80 yr. As compaction affects the lower part of the well-laminated section of the sediment (i.e., the sediment age is higher than estimated from the sedimentation rate in the upper part of the core, *see* Fig. 2), we assumed for modeling purposes that the mass movement was deposited about 100 years ago (*see* the next section). This also agrees reasonably well with the age determined by varve counting (Fig. 2).

Three different sections can be distinguished in the porosity profile (Fig. 2): a high water-content section at the top of the analyzed sediment column, a constant porosity section related to well-laminated sediments, and a section of decreasing porosity close to the depth range of the mass movement.

Table 2. Measured ^{137}Cs and ^{210}Pb activities per unit mass of sediment, ^{210}Pb activities corrected for in situ production ($^{210}Pb_u$) and estimated sediment age. The two ^{137}Cs activity peaks for Tschernobyl (1986) and the nuclear bomb tests in the 1960s are highlighted in bold. Even in the lowermost part of the profile the ^{137}Cs and ^{210}Pb ages are in reasonable agreement and deviate for less than 25% from each other.

z (m)	^{137}Cs (Bq kg ^{1})	^{210}Pb (Bq kg ^{1})	$^{210}Pb_u$ (Bq kg ^{1})	^{137}Cs age (yr)	^{210}Pb age (yr)
0.01	429±48	276±34	223±24	1	2
0.02	520±60	309±50	267±36	3	3
0.03	568±69	287±70	240±50	4	5
0.04	607±70	222±47	194±33	6	6
0.06	645±78	278±76	221±55	10	9
0.07	596±69	280±55	246±39	11	11
0.08	678±77	222±44	177±31	13	13
0.09	596±69	280±55	246±39	15	14
0.10	806±92	210±49	157±35	17	16
0.11	906±103	212±50	156±35	18	17
0.12	731±84	158±40	111±29	**19**	19
0.13	887±100	183±38	142±27	21	20
0.14	524±60	152±38	111±27	23	22
0.15	180±23	148±42	112±30	26	23
0.16	123±16	156±41	112±29	28	25
0.17	117±15	200±39	149±28	30	27
0.18	103±14	179±43	135±31	32	28
0.19	74±10	165±33	126±24	34	30
0.20	77±16	203±65	160±47	36	31
0.21	70±8	151±25		39	33
0.22	62±18	152±85	122±62	41	34
0.23	77±14	153±56	115±41	43	36
0.24	102±21	137±63	122±46	**45**	38
0.25	69±24			47	39
0.26	52±7	161±44	115±32	49	41
0.28	25±11	120±103	85±74	54	44
0.29	21±5	139±38	91±27	56	45
0.32		182±62	134±45	62	50
0.33		136±56	58±40	65	52
0.34		160±47	98±34	67	53
0.36		120±56	61±41	71	56
0.40		178±53	94±38	80	63
0.42		93±52	9±37	84	66
0.44		103±46		88	69
0.46		124±51	38±37	93	72
0.48		120±41	30±30	97	75
0.50		125±48	59±35	101	78

The water content in the upper 12 cm (Fig. 2, first section, blue) reaches 94%, but the section also contains two local porosity minima at approximately four centimeters and at 12 cm. The first minimum is most probably the result of water loss from the sediment core during transportation from Sweden to Switzerland (consistent with the presence of water at the bottom of the shipping containers). The second minimum seems to be related to the stepwise change in the measured $^{3}He/^{4}He$ ratio profile at about the same depth (Fig. 3C). The change in the shape of the porosity and $^{3}He/^{4}He$ profiles over this depth range supports the hypothesis that a slight difference in solute transport properties of the pore space may be present at the interface of the first and second sections.

Modeling the noble-gas concentrations in the sediment column

In a conceptual modeling exercise, we aim to assess the properties of a sediment column with respect to the solute

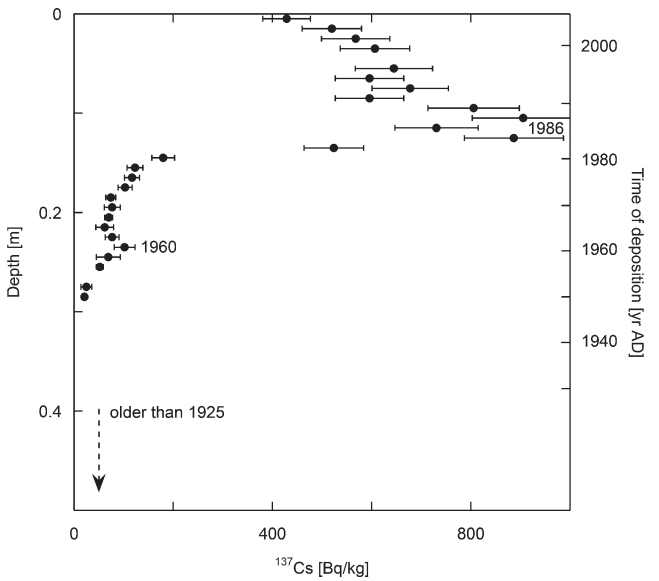

Fig. 5. ^{137}Cs activity measurements from a second core taken at the same location as the one taken for noble gas analysis. The ^{137}Cs activity peaks for Tschernobyl in 1986 and the nuclear tests in the 1960s are identified well at depths of 12 cm and 24 cm, respectively.

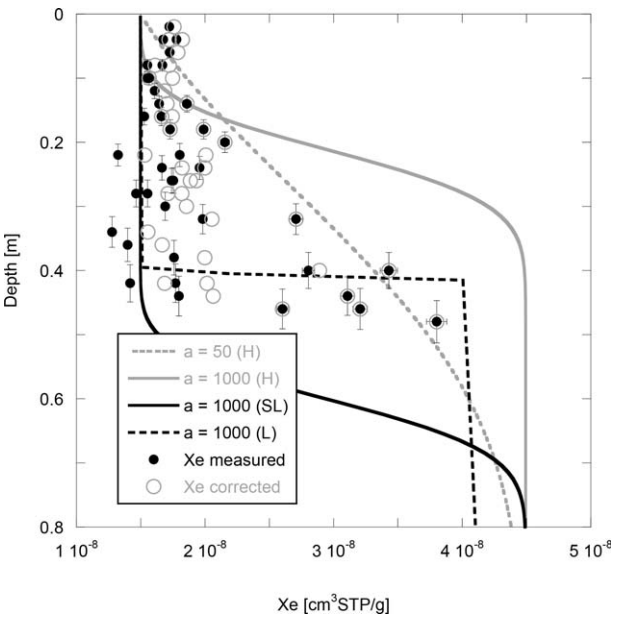

Fig. 6. Results for the diffusion model applied to a constant initial Xe concentration profile (300% saturation) considering different effective diffusivity profiles: homogeneous (H), step like (SL), and layer (L). The simulation time span (t) was set to 100 yr and different values for the attentuation parameter a (*see* Eq. 2) were used. Modeling the degassing corrected concentrations of He and Ne would result in an even stronger suppression of diffusive transport (not shown). The Xe concentrations corrected for possible degassing effects are shown as gray circles. As Xe is a large and heavy gas species, it is rather soluble. Differences between corrected and uncorrected Xe concentrations are, therefore, small and do not significantly influence the results of the modeling exercise. It should be noted that the sample with the highest Xe concentration of 5.90×10^{-8} cm^{3}STP g^{-1} (SE,331,28701, Table 1) is not within the plotted range.

transport enabling the conservation of sharp (noble gas) concentration gradients as found in the Stockholm Archipelago. We applied the advection/diffusion model of Strassmann et al. (2005) to analyze the vertical solute transport in a sediment column which consists of two sedimentologically different compartments representing the textural changes in the investigated sediment core as the result of the deposition of the mass movement unit at 40 cm. We systematically varied the transport characteristics (i.e., the effective diffusivity) in the upper (0 40 cm) and the lower (> 40 cm) compartments to conceptually describe the physical conditions that lead to the observed conservation of concentration excesses. In our analysis, we preset the solute concentrations over the entire modelled sediment column and let the solute transport operate over the given spatial and temporal scales.

To assess the solute transport within the sediment column by numerical modeling, the initial noble-gas concentration in the sediment column was set to 300% of the expected saturation concentrations with respect to the local temperature and salinity conditions (T 4°C, S 11 g kg^{-1}). At the upper boundary, located at the sediment/water interface, atmospheric equilibrium concentrations were held constant for the entire simulation. At the lower boundary, below the sedimentological intrusion, the concentration was set to a constant value of 300% of the saturation value. The relevant time span for the simulation of the diffusive transport of solutes in the pore space was set to 100 yr. A constant sedimentation rate of 4 mm/a was set considering the thickness of the undisturbed sediment section (40 cm) and the time span of the simulation.

To fit the model parameter a, which describes the diffusivity attenuation, to the measured concentration data, a standard least-squares method was chosen (Lyons 1991). Due to its larger solubility, Xe is less affected by degassing than the other lighter noble gases (Fig. 3B) and the measured Xe concentrations in the upper part of the core agree with the expected equilibrium concentrations. We, therefore, chose Xe as the target of our modeling exercise. In Fig. 6, the measured and corrected Xe concentrations are compared. In general, the measured Xe concentration profile deviates only slightly from the profile obtained after correction for degassing. The use of corrected concentrations, therefore, cannot significantly improve the estimation of a. Hence, we decided to use the Xe measurements with no correction for degassing as a reference concentration profile for the least-squares fitting process to analyze the solute transport in the sediments and to determine the effective diffusivity.

The modeling results for a homogeneous attenuation of effective diffusivity show that the measured (Xe) supersaturations just above and below the upper boundary of the mass movement in a depth range of about 35 50 cm *cannot* be

reasonably reproduced within the respective depth interval even if the effective diffusivity is strongly attenuated (Fig. 6). The attenuation parameter a in Eq. 2 needs be set to a value of ≈ 1000 (Fig. 6, solid gray line) to adequately maintain the step-like concentration increase for the simulated time period of 100 yr. However, as a result of the overall solute transport, the higher concentration initially set in the mass movement propagates toward the sediment/water interface and the modeling results do not match the experimental data. As such upward movement of the Xe supersaturation is not observed in the measured data, we conclude that the transport properties of the sediments above and below a depth of about 40 cm (the depth of the mass movement) are different that is, the solute transport below 40 cm is strongly attenuated.

The outcome of the numerical modeling considering a homogeneous attenuation of effective diffusivity indicates that structural changes in the sediments that constrain the local solute transport need to be considered. To this end, we used a step-like effective diffusivity profile by setting a 1 in the uppermost 40 cm and a 1000 below this depth threshold. The results of the adapted simulation reproduce better the Xe concentrations measured in the laminated sediment section (Fig. 6, solid black line). It should be noted that the original implementation of the solute transport model by Strassmann et al. (2005) cannot handle time-dependent effective diffusivity profiles. Therefore, the model starts with a much higher effective diffusivity in the mass movement which is slowly buried into the sediment column until it reaches its present depth of 40 cm. In the upper part of the mass movement, the modeled Xe super-saturation is transported toward the sediment/water interface much more efficiently than in reality. As a consequence, the modeled Xe concentration increase is rather smooth and is displaced for about 15 cm below the expected depth.

An even better fit to the measured data can be achieved by setting a 1000 only for a 1 cm-thick layer below a depth of 40 cm, whereas in the remaining sections of the sediment column a 1 (i.e., by separating two sediment compartments by a rather impermeable layer; Fig. 6, dashed black line). The layer of lower effective diffusivity acts as a barrier ("artificially" kept at a constant depth) modulating the release of Xe from the mass movement into the laminated section. The resulting concentration profile is based on the arbitrary assumption of the existence of a less permeable sediment layer. However, this assumption is in line with the general idea that the sediment structure in the depth range of the mass movement limits the fluid transport.

Such attenuation of the effective diffusivity indicates that only a relatively small fraction of the original noble-gas excess has been removed from the mass movement during 100 yr. Although caution needs to be exercised in drawing final conclusions, we reason, both from the experimental data and the modeling exercise (Fig. 6), that the effective diffusivity, $D_{\mathrm{eff},i}$, near the mass movement is about three orders of magnitude smaller than the diffusivity of Xe in bulk water ($D_{\mathrm{mol,Xe}} \approx 7.8 \times 10^{-10}\ \mathrm{m^2\ s^{-1}}$).

Consequently, our finding shows that the sediment structure i.e., the observed mass movement may significantly attenuate the effective diffusivity of solutes within the pore space of unconsolidated sediments even if the sediments have relatively high porosities (*see* also Brennwald et al. 2004; Strassmann et al. 2005; Pitre and Pinti 2010). Our results provide evidence that such horizontal barriers are effective in suppressing apparently diffusive transport, which might even become virtually negligible, possibly limiting solute exchange within the pore space for centuries or even longer.

Discussion

Numerical modeling of the solute transport and terrigenic He emanation suggest that the effective diffusivity in the pore space is strongly attenuated within the mass movement or at its upper end. Such low-diffusive behavior lets us speculate that a "closed" (or "separated") pore space, in which virtually no macroscopic diffusion alters the concentration profiles over time, could be present in the sediment column. The observed lower porosity near the mass movement (about 5% lower than that in the overlying sediment column; Fig. 2) seems to be indicative of a sediment-controlled diffusion barrier. Therefore, the hypotheses that relate the attenuation of the effective diffusivity to mineral formation, to mineral realignment, or to the existence of "dead" pores (Brennwald et al. 2013) are still viable options that are supported by the observed changes in the porosity profile.

However, it does not seem realistic to justify the observed attenuation of effective diffusivity in the shallow sediments of the Stockholm Archipelago only by considering diffusion in the pore water phase of the sediments, as our study implies an attenuation of the effective diffusivity which is much larger than the attenuation by "tortuosity effects" reported by other surveys (e.g., Boudreau 1986; Maerki et al. 2004). In fact, the extent of the compaction and cementation of the sediment resulting in a tortuosity which could reduce the effective diffusivity by three orders of magnitude requires considerably more time (several millennia) than the age of the sediment studied here (a few decades).

Conceptual model

To explain conceptually the observed strong attenuation of the solute transport into the sediment pore space (as shown exemplarily for He and Xe), we hypothesize that a mass movement from the air/water interface occurred in which a significant amount of air (as bubbles) was embedded (Brennwald et al. 2013). Such a single event would limit the transport of noble gases within the pore space by confining the effective noble-gas exchange to the gas exchange

occurring through the molecular boundary between nonmobile gas bubbles and stagnant pore water. However, this scenario poses the question of whether gas bubbles might be expected to exist within the sediment matrix. The observed Xe supersaturation of about 200% (3×10^{-8} $cm^3STP\ g^{-1}$, *see* Table 1) would correspond to the incorporation of 0.34 $cm^3STP\ g^{-1}$ of unfractionated air. Because of the hydrostatic pressure exerted by the water column, the total pressure at the water/sediment interface at 36 m is approximately 4.6 atm. The in situ gas volume in the sediment per unit mass of pore water is, therefore, $\approx 7.3\times10^{-2}$ $cm^3\ g^{-1}$. To dissolve this amount of air (N_2 amount per unit mass of water: 0.27 $cm^3STP\ g^{-1}$) completely, a pressure of about 13 atm would be required, which exceeds the total pressure at the sampling site by a factor of over 2.5. It follows that the buried air in the mass movement cannot have dissolved completely, leaving gas bubbles trapped within the sediment matrix.

The presence of gas bubbles in the sediment implies the trapping of noble gases in these bubbles. Because noble gases are only slightly soluble, just a very small fraction of the noble gases will be dissolved in the pore water, where the solute diffusion occurs. The much larger noble-gas fraction trapped in the stationary nonmobile gas bubbles would not be available for diffusion within the pore space on a macroscopic level. The presence of gas bubbles in the sediment is, therefore, consistent with the very strong attenuation of effective noble-gas diffusivity in the sediment. However, the nature of the processes that keep air bubbles trapped in the sediment remains unknown. The same mechanism might also be involved in the strong attenuation of noble-gas diffusion observed in other sediments (e.g., Brennwald et al. 2004, 2005; Pitre and Pinti 2010; Tomonaga et al. 2014).

Discrepancies between theory and measured data a call for an open scientific discussion

Although the conceptual model presented in the previous section might be appealing, the latter implicitly assumes the existence of a free gas phase in the sediments for about 100 yr. Indeed, free gas phases in unconsolidated sediments occur often in response to local (biogenic) gas production (e.g., CH_4, CO_2, N_2) and might support the persistence of the bubbles included by the mass movement into the sediment column. The original noble-gas composition trapped in the bubbles is expected to change in time accordingly to the solubility of the considered species (i.e., producing elemental fractionation characterized by a systematic depletion in heavier noble gases; e.g., Holocher et al. 2003). However, the measured atmospheric noble-gas concentrations are not fractionated (i.e., the elemental composition is very close to that of atmospheric air), indicating that virtually no secondary gas exchange occurred. Thus, the noble-gas saturation pattern suggests that a free gas phase existed for about 100 yr without being subject to any significant exchange process that could have modified the initial gas composition.

Further, without a strong attenuation of dissolved noble gas diffusion in the sediments, the kinetic isotope fractionation produced by the bubble/water exchange during the mass movement event would have been be replaced by air-saturated isotope ratios within a time span of 100 yr. As the ratio of the diffusion rates of the Ne isotopes ($D_{^{20}Ne}/D_{^{22}Ne}$ 1.010, Tyroller et al. 2014) is smaller than the one for the Ar isotopes ($D_{^{36}Ar}/D_{^{40}Ar}$ 1.055), the kinetic isotope fractionation during bubble/water exchange is expected to be larger for Ar than for Ne. However, the observed fractionations relative to the atmospheric equilibrium ratios of 0.8% for $^{20}Ne/^{22}Ne$ and 0.3% for $^{36}Ar/^{40}Ar$ show the opposite situation. This indicates that the kinetic fractionation has not attained a dynamic steady state between the gas phase and the water during the mass movement or the subsequent burial in the sediment.

Both observations (i.e., no elemental fractionation and no steady state in the gas exchange) set a challenge for the conventional concepts applied for the solute transport in the pore space and for the systematics of noble-gas geochemistry in aquatic systems. As a consequence, besides adsorption of noble-gases to the sediment matrix, none of the hypotheses proposed in Brennwald et al. (2013) (i.e., mineral formation/realignment, the existence of "dead" pores, or the presence of immobile gas bubbles) can be conclusively excluded from the mechanisms possibly responsible for the observed attenuation of diffusion.

Nevertheless, the concept that (abrupt) lithological changes in the sediment column can be associated with a strong attenuation of the vertical solute transport is supported by similar observations in Lake Issyk-Kul (Kyrgyzstan) (Brennwald et al. 2004) and in Lake Van (Turkey) (Cukur et al. 2013; Tomonaga et al. 2014). Although the present state of our knowledge does not seem to lead to a conclusive interpretation of the measured data, with this case study we hope to stimulate a constructive scientific discussion on the physical mechanisms involved in the preservation of the measured noble-gas concentration profiles.

Preservation of concentration signals

Our results demonstrate that the supersaturation of sediment pore water with dissolved noble gases generated by a single mass movement in the past can be stored as a step-like concentration feature for more than 100 yr. The mass movement or the gas bubbles induced by the mass movement in the sediments seems to restrict solute transport within the pore space, resulting in a reduction in the effective diffusivity by at least three orders of magnitude with respect to the diffusivity in bulk water. Such suppression of diffusion also allows us to speculate that the gases are partly trapped in closed pores or separate structures that are not

connected to the open pore space and are, therefore, do not form part of the diffusive-transport domain of the pore water where solutes are subject to diffusive exchange.

The observed degassing during sampling precludes further in-depth investigations of the origins of the measured excesses and the mechanisms responsible for the observed isotopic fractionation that leads to the distinct enrichment of light Ne and Ar isotopes near the mass movement below 40 cm depth. However, the observed enrichment of light gas isotopes indicates that some kind of kinetic process controls the gas dissolution in response to the formation of the mass movement. Such degassing phenomenon can only be overcome by much faster sampling techniques, which are currently not available. An adaptation of the standard sampling technique of Brennwald et al. (2003) is needed to shorten the time necessary for high-resolution sampling in organic-rich sediments of high porosity.

Even though the details of the mechanisms resulting in the unexpectedly strong attenuation of the effective diffusivity of noble-gases in the pore space could not be resolved in this study, our results suggest that the attenuation of the effective diffusivity is related to the textural and formational properties of the sediment. The structural differences between the varved sediments and the mass-flow deposit are directly related to the concentrations and the isotopic signatures of the dissolved noble gases in the pore water. The trapping of noble gases in stationary gas bubbles is in conceptual agreement with our data. However, to fully elucidate the mechanisms that result in the strong attenuation of effective noble-gas diffusivity in the pore space that is observed on the macroscopic level, it would be necessary to focus more on the microscopic processes involved, along the lines of the work that has already successfully been conducted on groundwater to understand how excess air is formed in porous media (Holocher et al. 2003; Klump et al. 2007, 2008).

Significance to Aquatic Environments

Our results add further evidence to the observation that certain types of sediment can conserve noble-gas concentrations for a very long time, as solute transport is massively attenuated (Brennwald et al. 2004; Strassmann et al. 2005; Tomonaga et al. 2014). This illustrates how useful noble gases dissolved in the pore water of sediments can be in reconstructing paleoenvironmental conditions, using similar approaches to those used in analyzing and interpreting dissolved noble-gas concentrations in groundwater (Kipfer et al. 2002; Aeschbach-Hertig and Solomon 2013).

The observed noble-gas excess allows the origin of the sediment mass in which it is contained to be identified as being near the air/water interface, as the noble-gas surplus has to originate in the atmosphere. Hence, atmospheric noble gases have the potential to identify mass movements released from shallow water depths.

References

Aeschbach-Hertig, W., F. Peeters, U. Beyerle, and R. Kipfer. 1999. Interpretation of dissolved atmospheric noble gases in natural waters. Water Resour. Res. **35**: 2779-2792. doi: 10.1029/1999WR900130

Aeschbach-Hertig, W., and D. K. Solomon. 2013. Noble gas thermometry in groundwater hydrology, p. 81-122. *In* P. Burnard and J. Hoefs [eds.], The noble gases as geochemical tracers. Advances in isotope geochemistry. Springer.

Appleby, P. G. 2001. Chronostratigraphic techniques in recent sediments, p. 171-201. In W. M. Last and J. Smol [eds.], Basin analysis, coring, and chronological techniques, v. 1. Tracking environmental change using lake sediments. Kluwer.

Appleby, P. G., and F. Oldfield. 1978. The calculation of lead-210 dates assuming a constant rate of supply of unsupported ^{210}Pb to the sediment. CATENA **5**: 1-8. doi: 10.1016/S0341-8162(78)80002-2

Ballentine, C. J., R. Burgess, and B. Marty. 2002. Tracing fluid origin, transport and interaction in the crust, p. 539-614. *In* D. Porcelli, C. Ballentine and R. Wieler [eds.], Reviews in mineralogy and geochemistry, v. 47. Noble gases in geochemistry and cosmochemistry. Mineralogical Society of America, Geochemical Society.

Berner, R. 1975. Diagenetic models of dissolved species in the interstitial waters of compacting sediments. Am. J. Sci. **275**: 88-96. doi:10.2475/ajs.275.1.88

Beyerle, U., W. Aeschbach-Hertig, D. M. Imboden, H. Baur, T. Graf, and R. Kipfer. 2000. A mass spectrometric system for the analysis of noble gases and tritium from water samples. Environ. Sci. Technol. **34**: 2042-2050. doi: 10.1021/es990840h

Boudreau, B. P. 1986. Mathematics of tracer mixing in sediments. Am. J. Sci. **286**: 161-238. doi:10.2475/ajs.286.3.161

Brennwald, M. S., N. Vogel, Y. Scheidegger, Y. Tomonaga, D. M. Livingstone, and R. Kipfer. 2013. Noble gases as environmental tracers in sediment porewaters and in stalagmite fluid inclusions, p. 123-153. In P. Burnard and J. Hoefs [eds.], The noble gases as geochemical tracers. Advances in isotope geochemistry. Springer.

Brennwald, M. S. 2004. *The Use of Noble Gases in Lake Sediment Pore Water as Environmental Tracers*. Diss. ETH Nr. 15629, ETH Zürich.

Brennwald, M. S., M. Hofer, F. Peeters, W. Aeschbach-Hertig, K. Strassmann, R. Kipfer, and D. M. Imboden. 2003. Analysis of dissolved noble gases in the pore water of lacustrine sediments. Limnol. Oceanogr.: Methods **1**: 51-62. doi:10.4319/lom.2003.1.51

Brennwald, M. S., D. M. Imboden, and R. Kipfer. 2005. Release of gas bubbles from lake sediment traced by noble gas isotopes in the sediment pore water. Earth Planet. Sci. Lett. **235**: 31-44. doi:10.1016/j.epsl.2005.03.004

Brennwald, M. S., and others. 2004. Atmospheric noble gases in lake sediment pore water as proxies for environmental change. Geophys. Res. Lett. **31**: L04202. doi:10.1029/2003GL019153

Cukur, D., S. Krastel, Y. Tomonaga, M. Çağatay, and A. Meydan. 2013. Seismic evidence of shallow gas from Lake Van, eastern Turkey. Mar. Pet. Geol. **48**: 341-353. doi:10.1016/j.marpetgeo.2013.08.017

Dyck, W., and F. Da Silva. 1981. The use of ping-pong balls and latex tubing for sampling the helium content of lake sediments. J. Geochem. Explor. **14**: 41-48. doi:10.1016/0375-6742(81)90102-3

Grathwohl, P. 1998. Topics in environmental fluid mechanics, v. 1. Diffusion in natural porous media. Kluwer.

Holocher, J., F. Peeters, W. Aeschbach-Hertig, W. Kinzelbach, and R. Kipfer. 2003. Kinetic model of gas bubble dissolution in groundwater and its implications for the dissolved gas composition. Environ. Sci. Technol. **37**: 1337-1343. doi:10.1021/es025712z

Holzner, C. P., D. F. McGinnis, C. J. Schubert, R. Kipfer, and D. M. Imboden. 2008. Noble gas anomalies related to high-intensity methane gas seeps in the Black Sea. Earth Planet. Sci. Lett. **265**: 396-409. doi:10.1016/j.epsl.2007.10.029

Horseman, S., J. Higgo, J. Alexander, and J. Harrington. 1996. Water, gas and solute movement through argillaceaous media. Technical report, Paris.

Imboden, D. M. 1975. Interstitial transport of solutes in non-steady state accumulating and compacting sediments. Earth Planet. Sci. Lett. **27**: 221-228. doi:10.1016/0012-821X(75)90033-3

Kipfer, R., W. Aeschbach-Hertig, F. Peeters, and M. Stute. 2002. Noble gases in lakes and ground waters, p. 615-700. *In* D. Porcelli, C. Ballentine and R. Wieler [eds.], Reviews in mineralogy and geochemistry, v. 47. Noble gases in geochemistry and cosmochemistry. Mineralogical Society of America, Geochemical Society.

Klump, S., O. A. Cirpka, H. Surbeck, and R. Kipfer. 2008. Experimental and numerical studies on excess-air formation in quasi-saturated porous media. Water Resour. Res. **44**: W05402. doi:10.1029/2007WR006280

Klump, S., Y. Tomonaga, P. Kienzler, W. Kinzelbach, T. Baumann, D. Imboden, and R. Kipfer. 2007. Field experiments yield new insights into gas exchange and excess air formation in natural porous media. Geochim. Cosmochim. Acta **71**: 1385-1397. doi:10.1016/j.gca.2006.12.006

Lyons, L. 1991. A practical guide to data analysis for physical science students. Cambridge Univ. Press.

Maerki, M., B. Wehrli, C. Dinkel, and B. Müller. 2004. The influence of tortuosity on molecular diffusion in freshwater sediments of high porosity. Geochim. Cosmochim. Acta **68**: 1519-1528. doi:10.1016/j.gca.2003.09.019

Mamyrin, B. A., and I. N. Tolstikhin. 1984. Developments in geochemistry, v. 3. Helium isotopes in nature, 1st ed. Elsevier.

Meili, M., P. Jonsson, and R. Carman. 2000. PCB levels in laminated coastal sediments of the Baltic Sea along gradients of eutrophication revealed by stable isotopes (δ^{15}N and δ^{13}C). Ambio **29**: 282-287. doi:10.1579/0044-7447-29.4.282

Oxburgh, E. R., R. K. O'Nions, and R. I. Hill. 1986. Helium isotopes in sedimentary basins. Nature **324**: 632-635. doi:10.1038/324632a0

Ozima, M., and F. A. Podosek. 2002. Noble gas geochemistry, 2nd ed. Cambridge Univ. Press.

Pennington, W., T. G. Tutin, R. S. Cambray, and E. M. Fisher. 1973. Observations on lake sediments using fallout ^{137}Cs as a tracer. Nature **242**: 324-326. doi:10.1038/242324a0

Persson, J., and P. Jonsson. 2000. Historical development of laminated sediments an approach to detect soft sediment ecosystem changes in the Baltic Sea. Mar. Pollut. Bull. **40**: 122-134. doi:10.1016/S0025-326X(99)00180-0

Pitre, F., and D. L. Pinti. 2010. Noble gas enrichments in porewater of estuarine sediments and their effect on the estimation of net denitrification rates. Geochim. Cosmochim. Acta **74**: 531-539. doi:10.1016/j.gca.2009.10.004

Podosek, F. A., T. J. Bernatowicz, and F. E. Kramer. 1981. Adsorption of xenon and krypton on shales. Geochim. Cosmochim. Acta **45**: 2401-2415. doi:10.1016/0016-7037(81)90094-6

Podosek, F. A., M. Honda, and M. Ozima. 1980. Sedimentary noble gases. Geochim. Cosmochim. Acta **44**: 1875-1884. doi:10.1016/0016-7037(80)90236-7

Renkin, E. 1954. Filtration, diffusion, and molecular sieving through porous cellulose membranes. J. Gen. Physiol. **38**: 225-243. doi:10.1085/jgp.38.2.225

Ritchie, J. C., J. R. McHenry, and A. C. Gill. 1973. Dating recent reservoir sediments. Limnol. Oceanogr. **18**: 254-263. doi:10.4319/lo.1973.18.2.0254

Schwarzenbach, R. P., P. M. Gschwend, and D. M. Imboden. 2003. Environmental organic chemistry, 2nd ed. Wiley.

Stephenson, M., W. J. Schwartz, T. W. Melnyk, and M. F. Motycka. 1994. Measurement of advective water velocity in lake sediment using natural helium gradients. J. Hydrol. **154**: 63-84. doi:10.1016/0022-1694(94)90212-7

Strassmann, K., M. S. Brennwald, F. Peeters, and R. Kipfer. 2005. Dissolved noble gases in porewater of lacustrine sediments as palaeolimnological proxies. Geochim. Cosmochim. Acta **69**: 1665-1674. doi:10.1016/j.gca.2004.07.037

Tomonaga, Y., R. Blättler, M. S. Brennwald, and R. Kipfer. 2012. Interpreting noble-gas concentrations as proxies for salinity and temperature in the world's largest soda lake (Lake Van, Turkey). J. Asian Earth Sci. **59**: 99-107. doi:10.1016/j.jseaes.2012.05.011

Tomonaga, Y., M. S. Brennwald, and R. Kipfer. 2011a. An improved method for the analysis of dissolved noble gases in the pore water of unconsolidated sediments. Limnol. Oceanogr.: Methods **9**: 42-49. doi:10.4319/lom.2011.9.42

Tomonaga, Y., M. S. Brennwald, and R. Kipfer. 2011b. Spatial distribution and flux of terrigenic He dissolved in the

sediment pore water of Lake Van (Turkey). Geochim. Cosmochim. Acta **75**: 2848-2864. doi:10.1016/j.gca.2011.02.038

Tomonaga, Y., M. S. Brennwald, A. F. Meydan, and R. Kipfer. 2014. Noble gases in the sediments of Lake Van solute transport and palaeoenvironmental reconstruction. Quat. Sci. Rev. **104**: 117-126. doi:10.1016/j.quascirev.2014.09.005

Tyroller, L., M. S. Brennwald, L. Mächler, D. M. Livingstone, and R. Kipfer. 2014. Fractionation of Ne and Ar isotopes by molecular diffusion in water. Geochim. Cosmochim. Acta **136**: 60-66. doi:10.1016/j.gca.2014.03.040

Weiss, R. F. 1970. Helium isotope effect in solution in water and seawater. Science **168**: 247-248. doi:10.1126/science.168.3928.247

Zhou, Z., C. J. Ballentine, R. Kipfer, M. Schoell, and S. Thibodeaux. 2005. Noble gas tracing of groundwater/coalbed methane interaction in the San Juan Basin, USA. Geochim. Cosmochim. Acta **69**: 5413-5428. doi:10.1016/j.gca.2005.06.027

Acknowledgments

We thank Prof. Per Jonsson and the staff of the Department of Applied Environmental Science at Stockholm University for their great support during the expedition in the Stockholm Archipelago. Thanks are due to Nora Denecke for her pleasant company and support during the preparation and execution of the field work in Sweden. The authors are grateful for the improvement of the ^{137}Cs and ^{210}Pb dating provided by Marian Fujak. Thanks also two anonymous reviewers for their valuable comments on the manuscript and David M. Livingstone and Ryan North for helpful comments and editing assistance.

This research was made possible thanks to funding from the Swiss Science Foundation (SNF Grants 200020 109465, 200020 121853, 200021 124981, and 200020 143340) and the EU Seventh Framework Programme for Research and Technological Development (Marie Curie International Outgoing Fellowship, Contract PIOF GA 2012 332404).

Submitted 28 June 2014
Revised 16 November 2014
Accepted 31 October 2014

Associate editor: Josef D. Ackerman